Potential Flow Problems with Emphasis on the Surface-Source Method," *Computational Methods in Applied Mechanics and Engineering*, Vol. 5, 1975, pp. 145–196.

[6]Mikhlin, S. G., *Integral Equations and Their Applications to Certain Problems of Mechanics, Mathematical Physics and Engineering*, 2nd ed., Macmillan, New York, 1964.

[7]Isaacson, E., and Keller, H. B., *Analysis of Numerical Methods*, Wiley, New York, 1966.

Computation of Unsteady Supersonic Quasi-One-Dimensional Viscous-Inviscid Interacting Internal Flowfields

Timothy W. Swafford*
Mississippi State University,
Mississippi State, Mississippi 39762

Introduction

THE study and analysis of internal flows have received significant attention over the past several decades because the operation of many physical devices, particularly regarding aerospace-related hardware, depends on proper designs to achieve near-optimum operating characteristics. Examples of such devices include any configuration where the flow is confined and an exchange between pressure and kinetic energy is desired (e.g., engine inlets, wind tunnel diffusers, rocket nozzles, etc.). These devices can be geometrically complex as well as viscous-flow dominated. Moreover, certain configurations and conditions can result in unsteady flow.

In the past, the design of these devices has, for the large part, depended on empirically based methodologies. More recently, computational techniques have played an increasingly important role in the design process as hardware becomes less conservative and is required to operate near the edge of the design envelope. A thorough computational investigation of flowfields of this type requires solution of the full Reynolds-averaged, multidimensional, time-dependent Navier-Stokes equations. Because solutions to these equations provide essentially all pertinent flowfield parameters (assuming these solutions are of acceptable accuracy), it is possible to perform parametric studies of a proposed geometry/flowfield combination, which could, in turn, be used to reduce significantly the risk associated with new hardware design. Unfortunately, obtaining numerical solutions to these equations for complex geometries and unsteady flowfields is expensive and time consuming, even using today's largest and fastest supercomputers. Therefore, it is important to seek alternative means of performing compute-based studies of proposed new hardware designs.

The development of an engineering tool through which preliminary estimates of unsteady supersonic internal flow processes can be generated using available workstation-based hardware is the underlying mission of the present effort. The approach encompasses a viscous-inviscid interaction technique where the flowfield is separated into inviscid and viscous parts and the appropriate equation sets (corresponding to each region) are solved using a new interaction technique. The assumption is made that inviscid flow phenomena can be adequately represented using the unsteady, quasi-one-dimensional (Q1D) Euler equations, whereas viscous effects are accounted for using integral boundary-layer equations for unsteady, two-dimensional, turbulent flow. Under these assumptions, the objective of this Note is to demonstrate a new method for computing unsteady interactions whereby the inviscid and viscous equations are cast as a (single) coupled system of partial differential equations and solved simultaneously. This approach to computing unsteady viscous-inviscid interactions for internal flows differs from techniques previously reported, where each equation set is solved independently of the other; i.e., the coupling procedure was performed between the *solutions* of the equations *and not between the equations themselves.* Viscous-inviscid coupling at the equation level has been demonstrated by Drela and Giles[1] for two-dimensional laminar/turbulent airfoil flows, and excellent results were obtained using minimal computational resources.[1] However, the technique reported in Ref. 1 involved steady external flows, and the present effort attempts to apply the approach to unsteady internal configurations. The motivation behind the approach presented herein is the observation that coupling the solutions results in schemes that can have convergence difficulties.[2] Moreover, marching the equations simultaneously yields a time-accurate coupling for unsteady flows which is more straightforward than marching each equation set separately.[3] However, it must be emphasized that the validity of using the simplified equations is very problem dependent and, similar to other analytical/computational techniques, requires experience and engineering judgment with regard to whether the approach and/or computed solutions represent reality. No attempt is made at quantifying specific classes of problems for which the approach presented herein can be used.

Use of the Q1D assumption for internal flow analysis is certainly not new, and both viscous and inviscid techniques have been reported. For example, the method of Mays[4] was perhaps the first to investigate time-dependent, variable-area duct flows by numerically solving the unsteady, Q1D inviscid flow equations. For purely steady subsonic diffuser flows, Harsha and Glassman[5] developed a technique whereby the boundary-layer equations for turbulent flow were solved in a marching fashion by iterating on the pressure gradient required to satisfy mass conservation. White and Anderson[6] investigated steady, inviscid, Q1D nozzle flows by numerically solving the Euler equations. Adams et al.[7] and Varner et al.[8] solved the Q1D inviscid equations for supersonic mixed compression inlets using a split-characteristics approach designed to capture accurately moving shocks for investigating inlet unstart/restart. A technique similar to that presented herein was reported by Bussing and Murman,[9] where the unsteady Q1D Euler equations were solved by dividing the flow into viscous and inviscid regions and modifying the inviscid equations to account for the mass defect brought about by the presence of the boundary layer. However, boundary-layer parameters were computed in a separate program and consequently were not solved alongside the inviscid equations.

A generic geometric configuration for which the present analysis is applicable is shown in Fig. 1. Fundamental considerations to the approach taken herein are the assumptions that the flowfield within the confines of the channel is not fully developed and that an inviscid core of fluid exists and is allowed to interact with the viscous region near the wall. The displacement of mass brought about by the presence of this viscous region has a thickness of δ^*, defined by

$$\rho_e u_e \delta^* = \int_0^\infty (\rho_e u_e - \rho u)\, dy$$

This displacement of mass affects the available flow area and consequently is a primary mechanism through which the viscous-inviscid interaction proceeds.

It should be pointed out that the preceding expression for δ^* is exact for planar flow but is in error for axisymmetric flow. However, the preceding expression approaches the true mass-flow defect length for the axisymmetric case when the local body radius is large compared to the local boundary-layer thickness.[10] This is an important distinction[11] because for cases

Received Nov. 7, 1991; revision received July 20, 1992; accepted for publication July 21, 1992.

*Associate Professor, Engineering Research Center for Computational Field Simulation, P.O. Box 6176. Member AIAA.

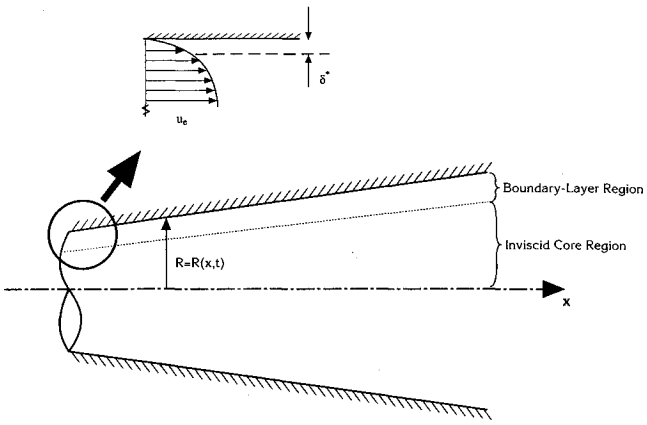

Fig. 1 Definitions of boundary-layer and inviscid core parameters.

where the boundary layer is thick compared to the local radius, δ^* will be in error and consequently any viscous-inviscid interaction technique that uses this parameter will also be in error. Therefore, the present analysis is further restricted to cases where the local boundary-layer thickness is small compared to the local body radius.

Analysis

An analysis methodology used to compute dynamic behavior of viscous internal flowfields must be capable of addressing time-varying area as well as unsteady boundary-layer effects. To that end, the equations that form the basis of the present approach are the unsteady Q1D Euler equations and the unsteady integral boundary-layer equations for turbulent flow. A derivation of the unsteady Q1D Euler equations valid for spatially and temporally varying area is given in Ref. 12. A description of the procedure that couples the unsteady Q1D Euler equations and the unsteady, integral boundary-layer equations for turbulent flow follows.

The Euler equations for unsteady, Q1D flow as used herein are given by[7,8,12]

$$\frac{\partial}{\partial t}(\rho_e A) + \frac{\partial}{\partial x}(\rho_e u_e A) = 0 \tag{1}$$

$$\frac{\partial}{\partial t}(\rho_e u_e A) + \frac{\partial}{\partial x}\left[(\rho_e u_e^2 + p_e)A\right] - p_e \frac{\partial A}{\partial x} = 0 \tag{2}$$

$$\frac{\partial}{\partial t}(E_e A) + \frac{\partial}{\partial x}\left[u_e(E_e + p_e)A\right] + p_e \frac{\partial A}{\partial t} = 0 \tag{3}$$

where ρ = density, u = velocity, p = pressure, E = total energy, t = time, and x = axial distance; subscript e has been added to the gas dynamic variables to denote "edge" values, taken to be those associated with the inviscid core. The area A (divided by 2π for axisymmetric flow) is given by

$$A = \int_f^g y^k \, dy \tag{3a}$$

where, by definition, limits f and g of the integral represent the lower and upper displacement surfaces associated with the channel wall(s). As a consequence, the flow of fluid between the f and g surfaces is inviscid, by definition. Note that for the axisymmetric case, y is to be interpreted as the radial coordinate and consequently $k = 1$, whereas in the planar case, y is the cartesian coordinate normal to the channel centerline in which case $k = 0$.

The equation set is completed by addition of the unsteady boundary-layer momentum and mean-flow kinetic energy integral equations for two-dimensional turbulent flow,[12]

$$\frac{\partial}{\partial t}(\rho_e u_e \delta^*) - u_e \frac{\partial}{\partial t}(\rho_e \theta_\rho) + \frac{1}{R^k}\frac{\partial}{\partial x}(\rho_e u_e^2 R^k \theta) + \rho_e u_e \delta^* \frac{\partial u_e}{\partial x} - \rho_e u_e^2 \frac{c_f}{2} = 0 \tag{4}$$

$$\frac{\partial}{\partial t}\left[\rho_e u_e^2(\theta + \delta^* - \theta_\rho)\right] + 2\rho_e u_e(\theta_\rho - \delta_u^*)\frac{\partial u_e}{\partial t} + \frac{1}{R^k}\frac{\partial}{\partial x}(R^k \rho_e u_e^3 \theta^*) + 2\rho_e u_e^2(\delta^* - \delta_u^*)\frac{\partial u_e}{\partial x} - 2\rho_e u_e^3 \frac{c_f D}{2} = 0 \tag{5}$$

where R is the local radius.

It should be noted that Eqs. (1-5) have been nondimensionalized using the parameters $\hat{R}_{\text{ref}}$, $\hat{\rho}_\infty$, and $\hat{U}_\infty$, where "^" denotes a dimensional quantity. The reference length ($\hat{R}_{\text{ref}}$) and "∞" conditions are typically taken to be those associated with the channel entrance. Similar to Eq. (3a), $k = 0$ for planar flow or 1 for axisymmetric flow. Also, definitions of integral lengths (θ, θ_ρ, etc.), skin friction (c_f), and dissipation integral (D) used in Eqs. (4) and (5) are given in Ref. 12.

The development of the coupled system of equations proceeds as follows. We can isolate the temporal derivatives by rewriting Eqs. (1-5) as

$$\frac{\partial}{\partial t}(\rho_e u_e \delta^*) - u_e \frac{\partial}{\partial t}(\rho_e \theta_\rho) = b_1 \tag{6}$$

$$\frac{\partial}{\partial t}\left[\rho_e u_e^2(\theta + \delta^* - \theta_\rho)\right] + 2\rho_e u_e(\theta_\rho - \delta_u^*)\frac{\partial u_e}{\partial t} = b_2 \tag{7}$$

$$\frac{\partial}{\partial t}(\rho_e A) = b_3 \tag{8}$$

$$\frac{\partial}{\partial t}(\rho_e u_e A) = b_4 \tag{9}$$

$$\frac{\partial}{\partial t}(E_e A) + p_e \frac{\partial A}{\partial t} = b_5 \tag{10}$$

where b_1 through b_5 are defined by referring to Eqs. (4), (5), (1), (2), and (3), respectively. Note that the equations are strongly coupled through the gas dynamic variables ρ_e, u_e, and p_e, as well as area A.

The approach taken herein to place the equations in a form amenable to solution follows that presented in Refs. 13 and 14, where the temporal derivatives are expanded and the ensuing terms algebraically manipulated to form a system of five simultaneous partial differential equations. These manipulations result in the following system of equations:

$$L \frac{\partial q}{\partial t} = b \tag{11}$$

where L is a 5×5 matrix, b the right-hand-side vector containing spatial derivatives, and q the dependent variable vector given by

$$q = (\rho_e \; u_e \; M_e \; \theta \; \bar{H})^T \tag{12}$$

Here M_e is the edge Mach number, θ the momentum thickness, and $\bar{H}$ a shape factor defined using integral lengths formed with kinematic properties,[11] i.e., $\bar{H} = \bar{\delta}^*/\bar{\theta}$ and $\bar{\delta}^* = \delta_u^*$.

The number of unknown parameters in Eq. (11) is ten, including those appearing in the vector b. Closure of the system is accomplished through the use of several auxiliary rela-

tions involving boundary-layer integral-length shape factors[11,12] (e.g., $H_{\delta^*}=\delta^*/\theta$, $H_{\theta^*}=\theta^*/\theta$, etc.) and the perfect gas equation of state. Details of the derivation of Eq. (11) along with the elements of L are given in Ref. 12. Specific auxiliary relations and correlations for c_f, H_{δ^*}, etc. are also given in Ref. 12 as well as other references.[11,15,16,17]

The previous system of equations has been solved numerically using semidiscretization in conjunction with a two-stage, explicit Runge-Kutta scheme employing first-order backward spatial differences. The use of backward spatial differencing stems from interrogating the eigenvalues of the matrix $L^{-1}N$, where elements of the matrix N are determined by rewriting Eq. (11) as

$$\frac{\partial q}{\partial t}+L^{-1}N\frac{\partial q}{\partial x}-L^{-1}d=0 \tag{13}$$

For supersonic flow, the eigenvalues of $L^{-1}N$ are positive (as well as real and distinct, at least for the cases investigated herein), thus permitting the use of one-sided differencing. Because of the algebraic complexity of the elements of L and N, analytic computation of these eigenvalues is not practical and thus must be computed numerically.[18] The time step is determined using the relation

$$\Delta t=(\mathrm{CFL})\frac{\Delta x}{\rho(L^{-1}N)} \tag{14}$$

where $\rho(L^{-1}N)$ is the spectral radius of the matrix $L^{-1}N$ and CFL is the maximum allowable Courant number for that particular numerical scheme and spatial difference operator; e.g., one for two-stage Runge-Kutta using first-order backward differences. For steady-state cases, convergence can be accelerated by using local time stepping where the solution at each point is advanced commensurate with flow conditions at that point. For transient cases, solutions are advanced using the maximum allowable Δt computed over all mesh points, often referred to as minimum time stepping.

Results

The following solutions are for both steady and unsteady supersonic flow. Because the methodology presented herein is new, test cases are restricted to simple configurations with relatively weak interaction, such that fundamental validity of the solution procedure can be established. All solutions were obtained using first-order backward differences with 51 equally spaced points in the axial direction. Computations were performed on a Silicon Graphics, Inc. (SGI) Personal IRIS 4d/30TG. The code was written such that computed quantities can be graphically displayed as the solution progresses, i.e., animated. Steady-state solutions were converged to machine epsilon (single precision) using the SGI Fortran 77 compiler (−O2 optimization), and convergence was obtained in 400–800 time cycles using a CFL of 0.9 with local time stepping. No attempt to optimize execution was made, resulting in a processing rate of approximately 1.6×10^{-3} CPU second per time step per grid point.

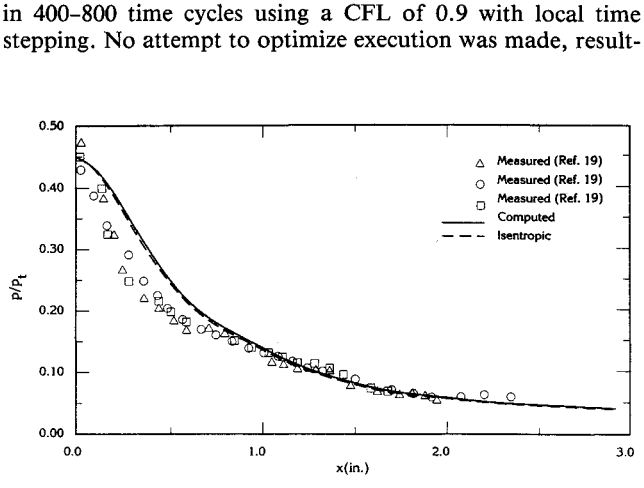

Fig. 2 Fifteen-degree supersonic nozzle total pressure ratio.

Steady Flow Case

As noted in Ref. 5, detailed measurements of flowfield parameters within internal configurations (subsonic and supersonic) are surprisingly sparse. However, conical converging-diverging 15 deg nozzle static pressure measurements[19] are compared with those computed using the present method in Fig. 2. Also shown for comparison is the pressure distribution obtained using one-dimensional isentropic relations between area and Mach number. Different symbols shown in Fig. 2 correspond to data obtained using various nozzle extensions for stagnation pressures between approximately 40 and 150 psia. The calculations were started from the geometric throat where the dependent variable vector was held fixed at estimated values of $M_e=1.13$, $\bar{H}=1.5$, and $\delta^*/R_{\mathrm{eq}}=0.0021$ (measured parameters were not available at this point). Conditions at the nozzle exit were computed using a second-order extrapolation for each dependent variable. Except for the throat region, where wall curvature is greatest, the comparison shown in Fig. 2 is considered good. Note that viscous effects are relatively small as indicated from the isentropic solution. A "traditional" boundary-layer solution was obtained using a code based on the steady integral boundary-layer equations [i.e., Eqs. (4) and (5) with the temporal derivatives discarded, essentially that reported in Ref. 11] and the computed core pressure distribution shown in Fig. 2. Although not shown here, boundary-layer parameters (e.g., skin friction, displacement thickness, etc.) as computed using the steady-state version[11] were essentially identical to those computed using the present interaction technique, indicating that the converged solution of the unsteady code recovered that calculated by the steady version. This result should be expected because of the weak interaction.

Unsteady Case—Sinusoidally Varying Inflow

To investigate the present technique's ability to compute an unsteady viscous-inviscid interaction, a straight-pipe configuration (with a length of 10 pipe radii) was contrived where upstream conditions are pulsated at some frequency. This was accomplished by sinusoidally varying the entrance Mach number to yield a mean value of 2 with a magnitude of oscillation of 0.2. Entrance values of density and velocity were varied commensurate with the Mach number (holding stagnation conditions constant) using isentropic relations, whereas momentum thickness and shape factor were held fixed. Conditions at the channel exit were extrapolated using second-order differencing. The reference Reynolds number at the pipe entrance was taken to be 5 million.

Illustrated in Fig. 3a are time histories of entrance (specified) and exit Mach number as computed by the present interaction technique for a nondimensional frequency (defined by $\omega=\hat{\omega}\hat{R}_{\mathrm{ref}}/\hat{U}_\infty$) of 0.1. The code was executed for 2000 time steps (CFL = 0.9), which resulted in approximately 550 time steps per inflow Mach number cycle. Also shown in Fig. 3a is the exit Mach number computed from the one-dimensional Euler equations, using MacCormack's scheme.[20] The phase shift of the computed exit Mach number compared to inviscid flow is the behavior one would expect because of blockage brought about by the presence of the boundary layer. Similar arguments can be made regarding the reduction of minimum and maximum Mach numbers given by the viscous solution compared to an inviscid flow.

Figure 3b presents axial distributions of displacement thickness at four different time levels within one inflow Mach number cycle. The particular times shown correspond to inflow Mach numbers of 2.0, 2.2, 2.0, and 1.8 (i.e., $t=125.7$, 141.4, 157.1, and 172.8 as shown in Fig. 3a). It can be seen that as the inflow Mach number goes through a cycle of oscillation, the displacement surface responds as a moving "wave," which increases and decreases corresponding to the imposed positive

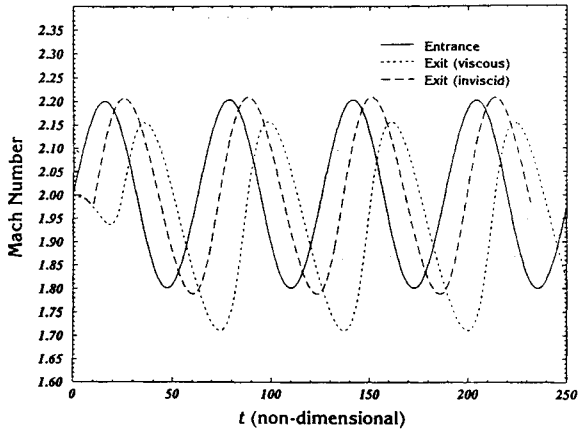

a) Entrance and exit Mach number

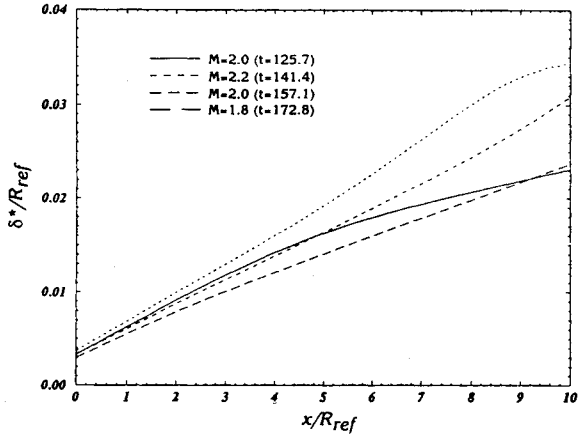

b) Snapshots of axial displacement thickness distributions

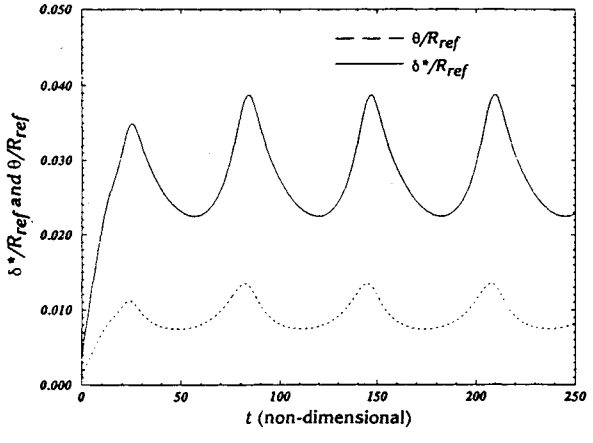

c) Exit displacement and momentum thickness

Fig. 3 Supersonic axisymmetric channel (oscillating inflow).

and negative axial pressure gradients, which, of course, are unsteady. The passing of this wave through the channel exit is illustrated more clearly in Fig. 3c, which shows time histories of exit displacement and momentum thickness. Although not shown here, other boundary-layer parameters (e.g., c_f) exhibit similar response to the imposed unsteady Mach number at the channel entrance.

It should be emphasized that the two-dimensionality of the inviscid core (e.g., Mach waves emanating from the displacement surface) has been lost. The degree to which these and other multidimensional effects may change the results shown here is not quantitatively known. However, because the maximum angular fluctuation exhibited by the displacement surface is approximately 0.10 deg, it can be argued that two-dimensional effects are neglible for this particular case. For conditions leading to larger fluctuations, multidimensional effects could become prominent. Therefore, care must be taken when using equations restricted to one-dimensional physics to address configurations where multidimensional effects may dominate.

Summary and Conclusions

Steady and unsteady quasi-one-dimensional internal supersonic flowfield calculations have been performed using a new viscous-inviscid interaction technique where the inviscid and viscous equations were directly coupled and solved simultaneously. The coupled system of equations was numerically solved using a two-stage Runge-Kutta scheme with first-order one-sided spatial differencing. Simple supersonic internal flow test cases were computed, and the basic capabilities of the computational procedure were demonstrated. Computations were performed using engineering workstation hardware where solutions could be graphically displayed as they were calculated.

As stated earlier, a major objective of the present analysis was to demonstrate that the equation sets governing viscous and inviscid flow could be cast as a coupled system of partial differential equations and solved simultaneously to produce results of engineering accuracy. Because this approach to computing viscous-inviscid interactions is relatively new, some rather fundamental test cases (exhibiting weak interaction) were attempted and reasonable results obtained. However, it is felt that this Note presents the first step toward further development of the new coupling technique. The ultimate utility of the method lies in its ability to address strong interaction cases (e.g., transonic flows with shocks and/or boundary-layer separation) because it is this type of interaction that tends to cause convergence problems regarding previous coupling methodologies. Therefore, before the present technique can be considered a viable alternative for strong interaction cases, it must be demonstrated to be more robust and yield comparable results for fewer resources than previous techniques.

Acknowledgments

This work was sponsored by NASA Lewis Research Center under Grant NAG3-1170 with Jacques C. Richard as Technical Monitor. This support is gratefully acknowledged. Additional coding to support real-time graphical display of computed solutions was performed by Michael L. Stokes of the MSU/ERC. This assistance is also gratefully acknowledged.

References

[1]Drela, M., and Giles, M. B., "Viscous-Inviscid Analysis of Transonic and Low-Reynolds Number Airfoils," *AIAA Journal,* Vol. 25, No. 10, 1987, pp. 1347–1355.

[2]Whitfield, D. L., Swafford, T. W., and Jacocks, J. L., "Calculation of Turbulent Boundary Layers with Separation and Viscous-Inviscid Interaction," *AIAA Journal,* Vol. 19, No. 10, 1981, pp. 1315–1322.

[3]Pirzadeh, S., "Three-Dimensional Unsteady Transonic Viscous-Inviscid Interaction," Ph.D. Dissertation, Mississippi State Univ., Mississippi State, MS, Dec. 1988.

[4]Mays, R. A., "Inlet Dynamics and Compressor Surge," AIAA Paper 69-484, June 1969.

[5]Harsha, P. T., and Glassman, H. N., "Analysis of Turbulent Unseparated Flow in Subsonic Diffusers," American Society of Mechanical Engineers, 76-FE-26, New York, Jan. 1976.

[6]White, M. E., and Anderson, J. D., Jr., "Application of MacCormack's Implicit Method to Quasi-One-Dimensional Nozzle Flows," AIAA Paper 82-0992, June 1982.

[7]Adams, J. C., Martindale, W. R., and Varner, M. O., "One-Dimensional Unsteady Modeling of Supersonic Inlet Unstart/Restart," AIAA Paper 84-0439, Jan. 1984.

[8]Varner, M. O., Martindale, W. R., Phares, W. J., Kneile, K. R., and Adams, J. C., Jr., "Large Perturbation Flow Field Analysis and Simulation for Supersonic Inlets," NASA CR 174676, Sept. 1984.

[9]Bussing, T. R. A., and Murman, E. M., "A One-Dimensional Unsteady Model of Dual Mode Scramjet Operation," AIAA Paper 83-

0422, Jan. 1983.
[10]Cebeci, T., and Smith, A. M. O., *Analysis of Turbulent Boundary Layers,* Academic Press, New York, 1974.
[11]Whitfield, D. L., "Integral Solution of Compressible Turbulent Boundary Layers Using Improved Velocity Profiles," Arnold Engineering Development Center TR-78-42, Arnold AFB, TN, Dec. 1978.
[12]Swafford, T. W., "Unsteady Viscous/Inviscid Interaction via Direct Coupling of the 1d-Euler and 2d-Integral Boundary-Layer Equations," Mississippi State Engineering and Industrial Research Station, Rept. MSSU-EIRS-ERC-90-1, Mississippi State, MS, March 1991.
[13]Swafford, T. W., and Whitfield, D. L., "Time-Dependent Solutions of Three-Dimensional Compressible Turbulent Integral Boundary-Layer Equations," *AIAA Journal,* Vol. 23, No. 7, 1985, pp. 1005-1013.
[14]Swafford, T. W., "Time-Dependent, Inverse Solution of Three-Dimensional, Compressible, Turbulent, Integral Boundary-Layer Equations in Nonorthogonal Curvilinear Coordinates," *Lecture Notes in Physics,* Vol. 218, Springer-Verlag, New York, 1985, pp. 541-545.
[15]Swafford, T. W., "Analytical Approximation of Two-Dimensional Separated Turbulent Boundary-Layer Velocity Profiles," *AIAA Journal,* Vol. 21, No. 6, 1983, pp. 923-926.
[16]Whitfield, D. L., Swafford, T. W., and Donegan, T. L., "An Inverse Integral Computational Method Compressible Turbulent Boundary Layers," *Recent Contributions to Fluid Mechanics,* edited by W. Haase, Springer-Verlag, New York, 1982, pp. 294-302.
[17]Donegan, Tracy, "Unsteady Viscous-Inviscid Interaction Procedures for Transonic Airfoil Flows," M.S. Thesis, Univ. of Tennessee, Knoxville, TN, Dec. 1983.
[18]Press, W. H., Flannery, B. P., Teukolsky, S. A., and Vettering, W. T., *Numerical Recipes: The Art of Scientific Computing,* Cambridge Univ. Press, New York, 1986, pp. 365-376.
[19]Back, L. H., Massier, P. F., and Gier, H. L., "Comparison of Measured and Predicted Flows Through Conical Supersonic Nozzles with Emphasis on the Transonic Region," *AIAA Journal,* Vol. 3, No. 9, 1965, pp. 1606-1614.
[20]MacCormack, R. W., "The Effect of Viscosity in Hypervelocity Impact Cratering," AIAA Paper 69-354, May 1969.

Axisymmetric Buckling of Antisymmetrically Laminated Spherical Caps

M. C. Narasimhan* and R. S. Alwar†
Indian Institute of Technology, Madras 600 036, India

Introduction

LAMINATED shells are finding increased applications in the aerospace, automobile, and power industries. These shells may be subjected to severe operational conditions, causing large deformations. There are not many investigations reported on the analysis of laminated spherical caps undergoing large axisymmetric deformations. Recently Xu[1] has investigated, using shallow shell theory, the large deformation problem of symmetrically laminated shallow spherical shells using the Bessel-Fourier series approach. The present investigation is concerned with the analysis, using deep shell theory, of large axisymmetric deformation behavior of antisymmetrically laminated cross-ply spherical shells. Estimates of snap pressures for symmetrically laminated caps using deep shell theory are compared with those of Xu.[1] Some new results with respect to antisymmetrically laminated caps are also presented.

Mathematical Formulation

Assuming the polar orthotropic cross-ply spherical cap to be undergoing moderately large axisymmetric deformations, the nonlinear strains and curvatures of the reference surface are given by

$$e_s^0 = \frac{du}{ds} + \frac{w}{R} + \frac{1}{2}\left\{\frac{dw}{ds} - \frac{u}{R}\right\}^2$$

$$e_\theta^0 = \frac{\cot\phi}{R}u + \frac{w}{R}$$

$$e_{sz}^0 = \left\{\frac{dw}{ds} + \alpha - \frac{u}{R}\right\}$$

$$\lambda_s^0 = \frac{d\alpha}{ds} - \frac{\alpha}{R}\left\{\frac{dw}{ds} - \frac{u}{RT}\right\} + \frac{1}{2}\frac{1}{R}\left\{\frac{dw}{ds} - \frac{u}{R}\right\}^2$$

$$\lambda_\theta^0 = \cot\phi\,\frac{\alpha}{R} \tag{1}$$

where u and w are displacements in the meridional and radial directions, respectively, and α the rotation of the normal (Fig. 1). R is the radius of the shell.

The governing equilibrium equations for axisymmetric deformations of laminated spherical shells are derived using virtual work principles and are given by

$$\frac{dN_s}{ds} + (N_s - N_\theta)\frac{\cot\phi}{R} + \frac{Q_s}{R} = \frac{N_s}{R}\left\{\frac{u}{R} - \frac{dw}{ds}\right\} - \frac{M_s}{R^2}\left\{\frac{u}{R} - \frac{dw}{ds} - \alpha\right\}$$

$$\frac{dM_s}{ds} + (M_s - M_\theta)\frac{\cot\phi}{R} - Q_s = \frac{M_s}{R}\left\{\frac{u}{R} - \frac{dw}{ds}\right\}$$

$$\frac{N_s + N_\theta}{R} - \frac{dQ_s}{ds} - Q_s\frac{\cot\phi}{R} = q - \frac{d}{ds}\left\{\left(N_s - \frac{M_s}{R}\right)\left(\frac{u}{R} - \frac{dw}{ds}\right)\right\} - \frac{\cot\phi}{R}\left\{\left(N_s - \frac{M_s}{R}\right)\left(\frac{u}{R} - \frac{dw}{ds}\right)\right\} - \frac{d}{ds}\left(\frac{M_s\alpha}{R}\right) - \frac{\cot\phi}{R^2}M_s\,\alpha \tag{2}$$

The relationship between the stress and moment resultants and generalized displacements, u, w, and α can be defined through the elements of the usual A-B-D stiffness matrices.

The three nonlinear equations of equilibrium and the five stress and moment resultants-displacement relations, along with the corresponding six boundary conditions, are linearized using the Taylor series approach.[2] These sets of linearized governing equations at each load step are then solved iteratively using a Chebyshev-Galerkin spectral method. The de-

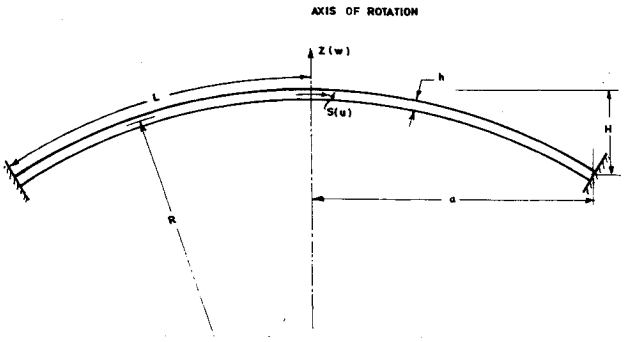

Fig. 1 Geometry and coordinate system for the shallow spherical cap.

Received Feb. 12, 1992; revision received July 10, 1992; accepted for publication July 27, 1992.

*Research Scholar, Department of Applied Mechanics.
†Professor, Department of Applied Mechanics.